AGU PUBLICATIONS

JGR

Journal of Geophysical Research: Space Physics

RESEARCH ARTICLE
10.1002/2016JA022967

Key Points:
- We statistically examine storm time solar wind and geophysical data as a function of UT of the storm peak
- There is a significant UT dependence to large storms; larger storms occur with a peak near 02:00 UT
- The difference in storm magnitude is caused by substorm activity and not by solar wind driving

Correspondence to:
R. M. Katus,
rkatus@umich.edu

Citation:
Katus, R. M., M. W. Liemohn, A. M. Keesee, T. J. Immel, R. Ilie, D. T. Welling, N. Y. Ganushkina, N. J. Perlongo, and A. J. Ridley (2016), Geomagnetic disturbance intensity dependence on the universal timing of the storm peak, *J. Geophys. Res. Space Physics*, *121*, 7561–7571, doi:10.1002/2016JA022967.

Received 18 MAY 2016
Accepted 26 JUN 2016
Accepted article online 29 JUN 2016
Published online 12 AUG 2016

Geomagnetic disturbance intensity dependence on the universal timing of the storm peak

R. M. Katus[1,2,3], M. W. Liemohn[2], A. M. Keesee[3], T. J. Immel[4], R. Ilie[2], D. T. Welling[2], N. Yu. Ganushkina[2,5], N. J. Perlongo[2], and A. J. Ridley[2]

[1]Department of Mathematics, Eastern Michigan University, Ypsilanti, Michigan, USA, [2]Department of Physics and Astronomy, West Virginia University, Morgantown, West Virginia, USA, [3]Department of Climate and Space Sciences and Engineering, University of Michigan, Ann Arbor, Michigan, USA, [4]Space Sciences Laboratory, University of California, Berkeley, California, USA, [5]Finnish Meteorological Institute, Helsinki, Finland

Abstract The role of universal time (UT) dependence on storm time development has remained an unresolved question in geospace research. This study presents new insight into storm progression in terms of the UT of the storm peak. We present a superposed epoch analysis of solar wind drivers and geomagnetic index responses during magnetic storms, categorized as a function of UT of the storm peak, to investigate the dependency of storm intensity on UT. Storms with *Dst* minimum less than −100 nT were identified in the 1970–2012 era (305 events), covering four solar cycles. The storms were classified into six groups based on the UT of the minimum *Dst* (40 to 61 events per bin) then each grouping was superposed on a timeline that aligns the time of the minimum *Dst*. Fifteen different quantities were considered: seven solar wind parameters and eight activity indices derived from ground-based magnetometer data. Statistical analyses of the superposed means against each other (between the different UT groupings) were conducted to determine the mathematical significance of similarities and differences in the time series plots. It was found that the solar wind parameters have no significant difference between the UT groupings, as expected. The geomagnetic activity indices, however, all show statistically significant differences with UT during the main phase and/or early recovery phase. Specifically, the 02:00 UT groupings are stronger storms than those in the other UT bins. That is, storms are stronger when the Asian sector is on the nightside (American sector on the dayside) during the main phase.

1. Introduction

It is well known that geomagnetic disturbances are governed by the dynamics of the interplanetary magnetic field (IMF) and solar wind. Changes in the north-south direction of the IMF B_z trigger geomagnetic activity; see *Dungey* [1961] and the reviews by *Gonzalez et al.* [1994, 1999]). IMF B_z causes dayside magnetic reconnection, which results in a magnetic pressure imbalance within the magnetosphere that propagates plasma Earthward through the plasma sheet and intensifies near-Earth space currents. If the southward IMF B_z is strong for a long interval (hours), then a geomagnetic storm can arise [e.g., *Gonzalez et al.,* 1994].

Diurnal effects can impact solar-terrestrial coupling. The terrestrial magnetic field is tilted at an angle of approximately 11° with respect to the rotational axis and offset from the center of the planet. The magnetic field is also complicated by crustal fields [*Mandea and Purucker*, 2005]. Semiannual variation is typically attributed to the Russell-McPherron effect. *Russell and McPherron* [1973] showed that angle between the terrestrial and solar magnetic fields affects the rate of reconnection. During equinoxes, the angle between the ecliptic plane and the magnetic field minimizes, which projects the Parker spiral onto the Earth's magnetic field producing a parallel component, allowing reconnection to occur. The enhancement of the southward IMF component (B_s) accounts for the observed higher geomagnetic activities in March and September since geomagnetic disturbances are related to B_s.

Longitudinal dependence of the geomagnetic response to solar wind driving is not very well understood. In particular, it is unclear whether the rotation of the magnetic poles around the geographic pole plays a role in storm dynamics. Some studies have examined how the tilt of the Earth with respect to the sun affects geomagnetic activity. For example, *Lyatsky et al.* [2001] tested the universal time (UT) variation of geomagnetic activity to show that geomagnetic activity is maximized when the nightside auroral zones of both hemispheres are in darkness (as happens during the equinoxes). They suggested

that during this time, no conducting path exists in the ionosphere to complete the currents required by solar wind-magnetosphere-ionosphere coupling, and therefore, more aurora is needed. *Perlongo and Ridley* [2016] proved significant hemispheric asymmetries based on idealize runs of the Global Ionosphere-Thermosphere Model (GITM). *Newell et al.* [2002] argued that the diurnal and semiannual variations of geomagnetic disturbances are due to the variations of the ionospheric conductivity in auroral zones. The ionospheric conductivity is an important factor for the current systems of asymmetric (ASYM) field [e.g., *Kamide and Fukushima*, 1971].

A data set that has been particularly insightful for revealing UT dependence is total electron content (TEC) derived from Global Positioning System measurements. For instance, *Foster et al.* [2005] used IMAGE data to show localized TEC enhancement over the American sector during strong storms, and *Coster et al.* [2007] found that storm enhanced density (SED) plumes are greatest in the American sector. *Immel and Mannucci* [2013] showed a storm time UT dependence in TEC and *Dst*. They confirmed that the American sector exhibits, on average, larger storm time enhancement in ionospheric plasma content, up to 50% in the afternoon middle-latitude region and 30% in the vicinity of the high-latitude auroral cusp, with largest effect in the Southern Hemisphere. *Astafyeva et al.* [2015] found significant TEC increases in different local time sectors at different UTs for the 17–18 March 2015 geomagnetic storm but enhancements around the same area of the Eastern Pacific region, which indicates a regional impact of storm drivers.

Huang [2013] conducted theoretical studies of ionospheric responses to geomagnetic storms with model simulations. They examined the disturbance dynamo intensity as a function of UT and season and found significant variation in the magnitude of these electric fields for similar activity levels.

Barakat et al. [2015] used the generalized polar wind model to simulate ionospheric outflow during the 28 September 2002 storm, close to equinox conditions. They focused on the effects of the offset between the geographic and the magnetic axes on the ionospheric ion outflow into the magnetosphere. They found that the diurnal modulation of the H+ total flux dominated the nonperiodic variations, because the H+ flux was near its limiting value. In contrast to H+ ions, the O+ flux was less than its limiting value. Therefore, the nonperiodic variations due to the other factors were comparable (though weaker than) with the diurnal quasi-sinusoidal oscillations of the O+ total hemispheric flux. They concluded that further study is required to investigate the consequences of this phenomenon on the magnetosphere's behavior.

While these studies provide breaking new work from an ionospheric point of view, further work is needed to understand the relationship between geomagnetic storms and terrestrial longitudinal configuration. *Saroso et al.* [1993] statistically examined UT variations in the *ap* and *Dst* indices. They found that (unlike *Dst*) the averaged *ap* values and the numbers of events of the *ap* greater than 30, 50, and 100 reach a minimum around 1030 UT or during the UT time interval 0900–1200. They also show that these values are correlated with the maximum value of the magnetic flux that occupies the nightside auroral oval. They conjecture that the modulation of $E \times B$ drift speed in the magnetosphere by the UT variation of the oval magnetic flux could be the source of the UT variation in the *ap* and the *Dst* indices.

This study continues these efforts by examining the UT control of storm intensity. We present a statistical study that examines several data sets that describe solar wind and geomagnetic activity in terms of the UT of the storm peak. In particular, it is shown that a strong increase in storm intensity occurs for events that peak between 00:00 and 04:00 UT. Solar wind biases are ruled out, and other possible causes are examined. Using auroral indices, such as *AU* and *AL*, we show that the magnitude enhancements are caused by heightened substorm activity.

2. Data Sets

Several indices have been developed to describe the magnitude of a geomagnetic storm using the geomagnetic north-south (*H*) component of the terrestrial magnetic field at low-to-middle latitudes. *Dst* is calculated from the hour average of four low-to-middle latitude magnetometers, approximately equally spaced in local time [*Sugiura and Kamei,* 1991]. This index is well correlated to solar wind parameters [e.g., *Burton et al.,* 1975; *O'Brien and McPherron,* 2000] and the total energy content of the ring current [*Dessler and Parker*, 1959; *Sckopke*, 1966; *Greenspan and Hamilton*, 2000; *Turner et al.,* 2001; *Liemohn and Kozyra*, 2003; *Jorgensen et al.,* 2004; *Ganushkina et al.,* 2006, 2012].

Table 1. The Number of Storms, Mean of the Peak, and Minimum *SYM-H* in Each UT Bin

UT Bin	Range	Number of Storms	<*SYM-H* Peak>	Min *SYM-H*
2 UT	[0–4) UT	40	−177 nT	−687 nT
6 UT	[4–8) UT	65	−152 nT	−391 nT
10 UT	[8–12) UT	59	−158 nT	−421 nT
14 UT	[12–16) UT	45	−123 nT	−315 nT
18 UT	[16–20) UT	40	−143 nT	−286 nT
22 UT	[20–24) UT	56	−131 nT	−410 nT
All UT	All UT	305	−147 nT	−687 nT

The *SYM-H* index provides a high-time resolution (1 min) alternative for *Dst* [*Iyemori*, 1990; *Iyemori et al.,* 1992]. The temporal resolution delivers critical information about physical processes that occur on time scales less than 1 h. There are differences between the *Dst* and *SYM-H* data sets [*Wanliss and Showalter*, 2006; *Katus et al.,* 2013], including up to 20% error during storm times [*Katus and Liemohn*, 2013]. *SYM-H* is calculated using six magnetometer stations that extend higher in latitude than those used for *Dst*. The largest difference between the measurements of *SYM-H* at each station is used to define the *ASY-H* index. *ASY-H* is typically used to describe the longitudinal asymmetry of the low-to-middle latitude disturbance, predominantly accredited to field-aligned and ionospheric currents that close the region 1 and the partial ring current [e.g., *Fukushima and Kamide*, 1973; *Crooker and Siscoe*, 1974, 1981; *Liemohn*, 2003; *Dubyagin et al.,* 2014].

The U.S. Geological Survey (USGS) also produces a 1 min low-latitude disturbance index [*Gannon and Love*, 2011], which we will refer to as the $USGS_{Dst}$. The $USGS_{Dst}$ index uses the same four low-latitude observatories as *Dst*. The difference is that the $USGS_{Dst}$ is calculated using the time and frequency space method described in *Love and Gannon* [2009]. They showed that the main field data reveal several sets of harmonics, which they used to remove the solar quiet time (*Sq*) variation.

The westward and eastward electrojets are described by the lower (*AL*) and upper (*AU*) auroral electrojet indices, respectively [e.g., *Davis and Sugiura,* 1966; *Mayaud*, 1980]. While a response in both *AU* and *AL* indicates increased potential-driven convection, a response in only the *AL* index describes the westward electrojet partially closing the substorm current wedge. Substorm activity is the mechanism of particle dissipation at polar latitudes, responsible for the aurora and subsequent intensification of the westward electrojet.

The geomagnetic storm-driving conditions are described using solar wind data as well as the IMF and electric field. IMF B_x, B_y, B_z, as well as the solar wind density, dynamic pressure, and electric field E_y are of particular importance. These parameters are typically used to predict the magnitude of a geomagnetic storm. In this study we used minimum variance, time-propagated ACE, WIND, and IMP8 solar wind data [*Weimer et al.,* 2003; *Weimer,* 2004] to maintain the minimum time delay error. These data sets are provided by OMNI in both low (1 h) and high (1 min) resolutions with varying ranges of availability.

3. Method

Examination of the UT control of storm intensity should be done statistically in order to determine the overall trend. Therefore, we began by creating a large database of 305 storms following the method of *Katus et al.* [2013]. To do this, we searched the *Dst* index from the years 1970 to 2012 for all of the intense ($Dst_{peak} \leq -100$ nT) storms. We then sorted the storms by the UT of the storm peak. Each UT bin is 4 h and described by the center value; thus, 2 UT contains all of the storms with Dst_{peak} times from 00:00 UT (included) to 04:00 UT (not included). The number of storms in each UT bin ranges from 40 to 65; the exact numbers are given in Table 1.

In this study we conduct a superposed epoch analysis of classified UT storm sets. The data are aligned into 15 min time steps using the storm peak as the epoch marker, placed at 24 h. The *SYM-H* data along the epoch timelines for each UT bin are shown in Figure 1. In these plots, the color bar describes the number of data points in each 10 nT by 15 min epoch time pixel. The black and pink lines show the mean and median *SYM-H* at each time step. The six mean curves as well as the mean curves for the 1 min $USGS_{Dst}$ and the 1 h *Dst* index are presented in Figures 2a, 2d, and 2g.

The color bar in Figure 1 shows the distribution of data at each epoch time step. This work statistically compares the distributions using two-sample *t* tests. In particular, the analysis tests whether the means of the distributions are statistically significantly different. This method requires the distributions to be approximately normally distributed.

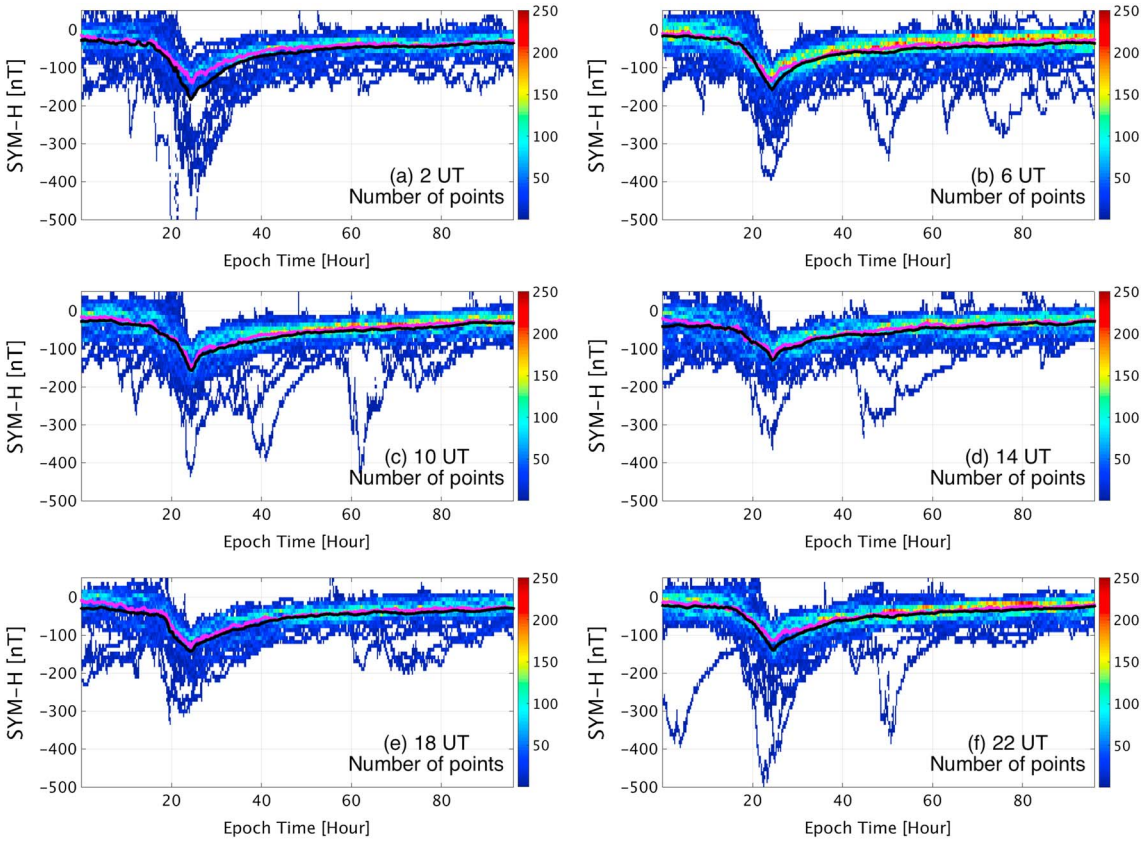

Figure 1. (a–f) *SYM-H* for all of the storms along the superposed epoch timeline. The storms are grouped by the UT of the storm peak. The color describes the number of data points in each 10 nT by 15 min time step.

A two-sample *t* test is a parametric test that compares two independent data samples. The purpose is to test the null hypothesis that the two data samples are from populations with equal means. The test statistic is calculated using the formula:

$$T = \frac{\overline{x} - \overline{y}}{\sqrt{\frac{s_x^2}{n} + \frac{s_y^2}{m}}} \tag{1}$$

where $\overline{x}$ and $\overline{y}$ are the sample means, s_x and s_y are the sample standard deviations, and n and m are the sample sizes of x and y, respectively. The null hypothesis is rejected if

$$|T| > t_{1-\alpha/2,v} \tag{2}$$

that is, if the absolute value of the test statistic is greater than a critical value (t) at a significance level (α), with degrees of freedom ($v = n + m - 2$). Critical values are provided in tables within many statistics books or online.

To simplify the result, the H value and P value were used. The H value defines the test decision for the null hypothesis. The value of $H = 0$ indicates that the two-sample t test does not reject the null hypothesis at a 5% significance level ($|T| < t_{1-\alpha/2,v}$). The value of $H = 1$ indicates that the t test rejects the null hypothesis ($|T| > t_{1-\alpha/2,v}$). The P value is then the probability that H was found by random chance. The P value is defined as the area under the normal distribution curve T outside of $t_{1-\alpha/2,v}$. Therefore, $H = 1$ with a small P value demonstrates a strong rejection of the null hypothesis, i.e., the means are statistically different.

In this study the H and P values are shown to simplify the explanation but are used to statistically determine whether the samples have equal means ($h = 0$) or not ($h = 1$). We require a 5% significance level. Additionally, it was assumed that the samples have equal variance. This is a reasonable assumption for most geophysical quantities and places only a mild constraint on result interpretation.

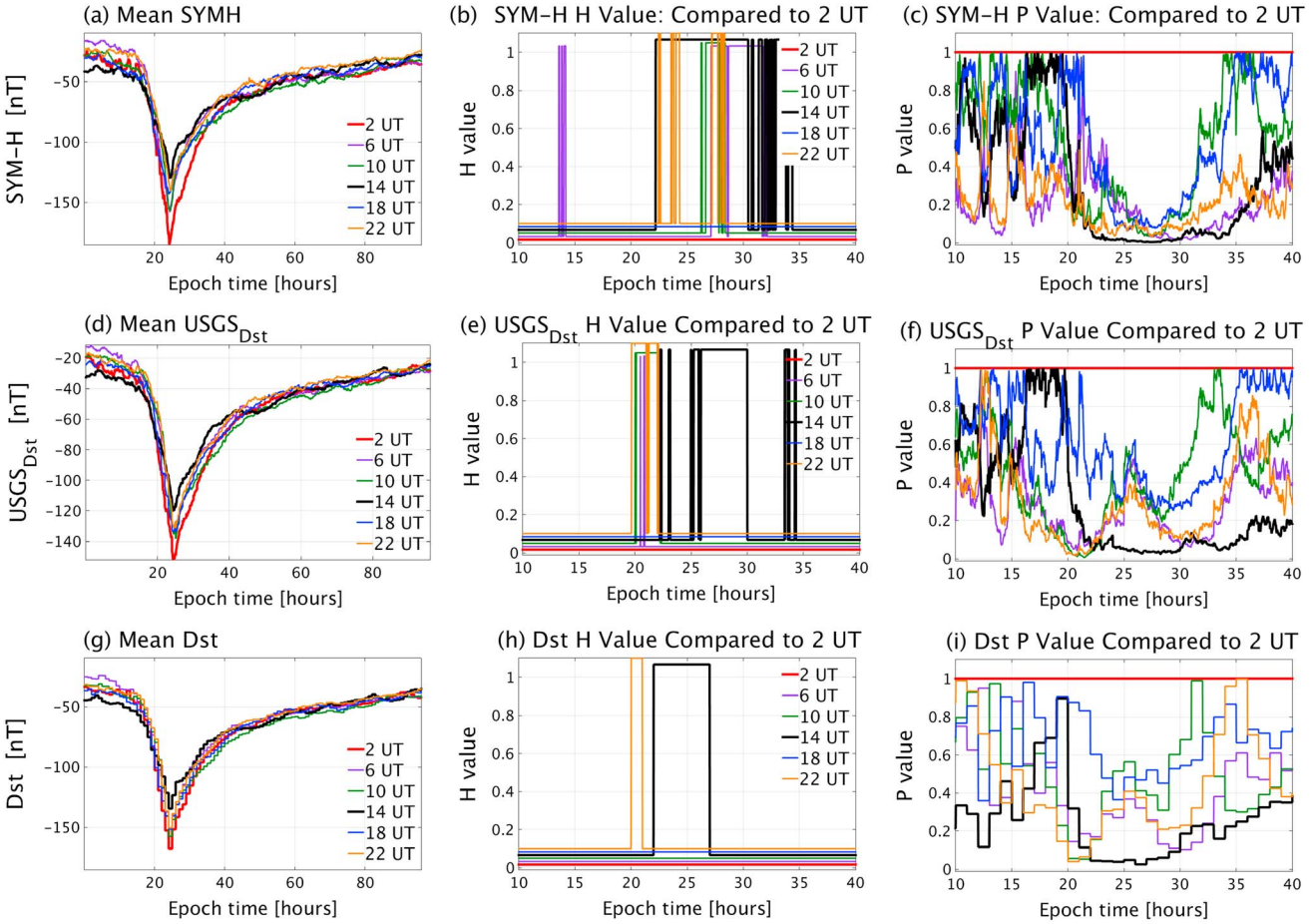

Figure 2. (a, d, and g) The mean *SYM-H* (top), USGS$_{Dst}$ (middle), and *Dst* (bottom) for each UT group of storms along the entire epoch timeline. (b, e, and h) The *t* test result, *H*, to accept (0) or reject (1) the null hypothysis that the means are the same along a shortened (10–40 h) epoch timeline to show the storm peak (near 24 h). The *t* test values are staggered by 0.1 to better show the UT bins. (c, f, and i) The *P* values associated with the test statistic.

In the following sections it is shown that the geomagnetic storm intensity is a function of the UT of the storm peak. To do this, the distribution of data at each point along the epoch timeline is shown to be approximately normal. It should be noted that while only *SYM-H* is shown, this step has been completed for each data set presented. The analysis of only the most relevant variables is presented in this study, and analysis of others was conducted but is not shown. The means of the distributions were then compared using the two-sample *t* test and the associated probability. These methods were also used to verify that the difference in storm intensity between UT bins did not originate in the solar wind. In fact, it is shown that differences in the storm magnitude are the product of enhanced storm time substorm activity during the main phase.

4. Results

Considering the distribution of the *SYM-H* index for each storm peak UT bin along the epoch timeline in Figure 1, the 2 UT bin has more super storms (defined by $Dst_{peak} \leq -250$ nT) than any other UT bin. In fact, Table 1 shows that while the 2 UT bin does not have an excessive number of storms, the minimum *SYM-H*$_{peak}$ is an extreme value, *SYM-H* = 687 nT. These super storms drive the average *SYM-H*$_{peak}$ down to −176.97 nT. That is |18 nT| larger than any other UT bin.

Table 2 presents the UT-dependent *SYM-H* as a function of a 3 month grouping, centered on the solstices and equinoxes. This table shows that regardless of the 3 month grouping, the average *SYM-H*$_{peak}$ 2 UT bin is typically more negative than the total average for the 3 month bin, the only exception being in one equinoctial

Table 2. The Mean of the Peak *SYM-H* in Each UT Bin Grouped by Month

	February–April	May–July	August–October	November–January
All storms	−147	−149	−143	−151
2 UT	−214	−193	−135	−167
6 UT	−165	−122	−150	−164
10 UT	−170	−154	−157	−134
14 UT	−102	−166	−120	−103
18 UT	−138	−124	−160	−147
22 UT	−107	−144	−133	−164

grouping. Furthermore, the average $SYM\text{-}H_{peak}$ 14 UT bin is typically less negative than the total average for that 3 month bin, the only exception being in one solstice grouping.

Figures 2a, 2d, and 2g show the average epoch timeline of each UT bin for (top) *SYM-H*, (middle) $USGS_{Dst}$, and (bottom) *Dst*. These plots demonstrate that the 2 UT bin is consistently more intense than any other bin regardless of the magnetometers or method used to calculate it. Furthermore, the 14 UT bin is consistently the least intense. To validate that the magnitude of the 2 UT bin is statistically different, we apply the *t* test.

Figure 2 also shows the *t* test results as *H* values (center column) and the associated probability *P* that the result is due to random chance (right column), for the three indices calculated for a reduced timeline (10–40 h of epoch time). It should be noted that the *H* values are staggered by 0.01 to make the lines easier to see. The figure compares the 2 UT bin to all other bins. Each colored line shows a comparison of the 2 UT *SYM-H* mean value against the *SYM-H* mean value from another UT bin as a function of epoch time. For two values to be identified as statistically significantly different, both the *H* value should be 1 and the *P* value should be below 0.05 for a given epoch time.

The plots in Figure 2 show *H* values of 1 and low *P* values for the time surrounding the storm peak (near the epoch time of 24 h). While the evidence is consistent for each of the three indices to some degree, it is more definitive for the higher resolution *SYM-H* and $USGS_{Dst}$ indices. The purple lines show the *t* test results of the 2 UT bin against itself, and the results are $H = 0$ and $P = 1$ everywhere, as expected. Most of the other lines

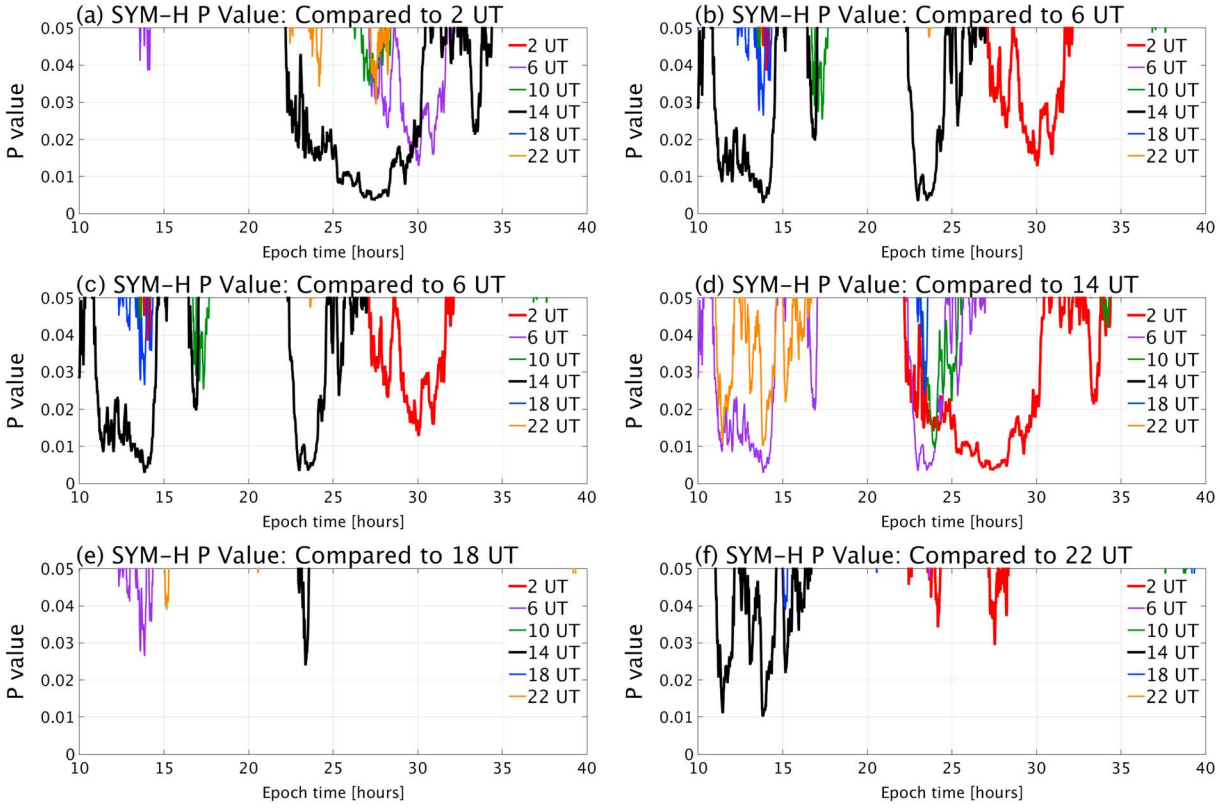

Figure 3. The probability (*P*) that differences in the mean *SYM-H* values along epoch time for each UT bin are due to random chance. The *P* values are only shown if they are less than 0.05 associated with $H = 1$ for each UT bin compared to each other.

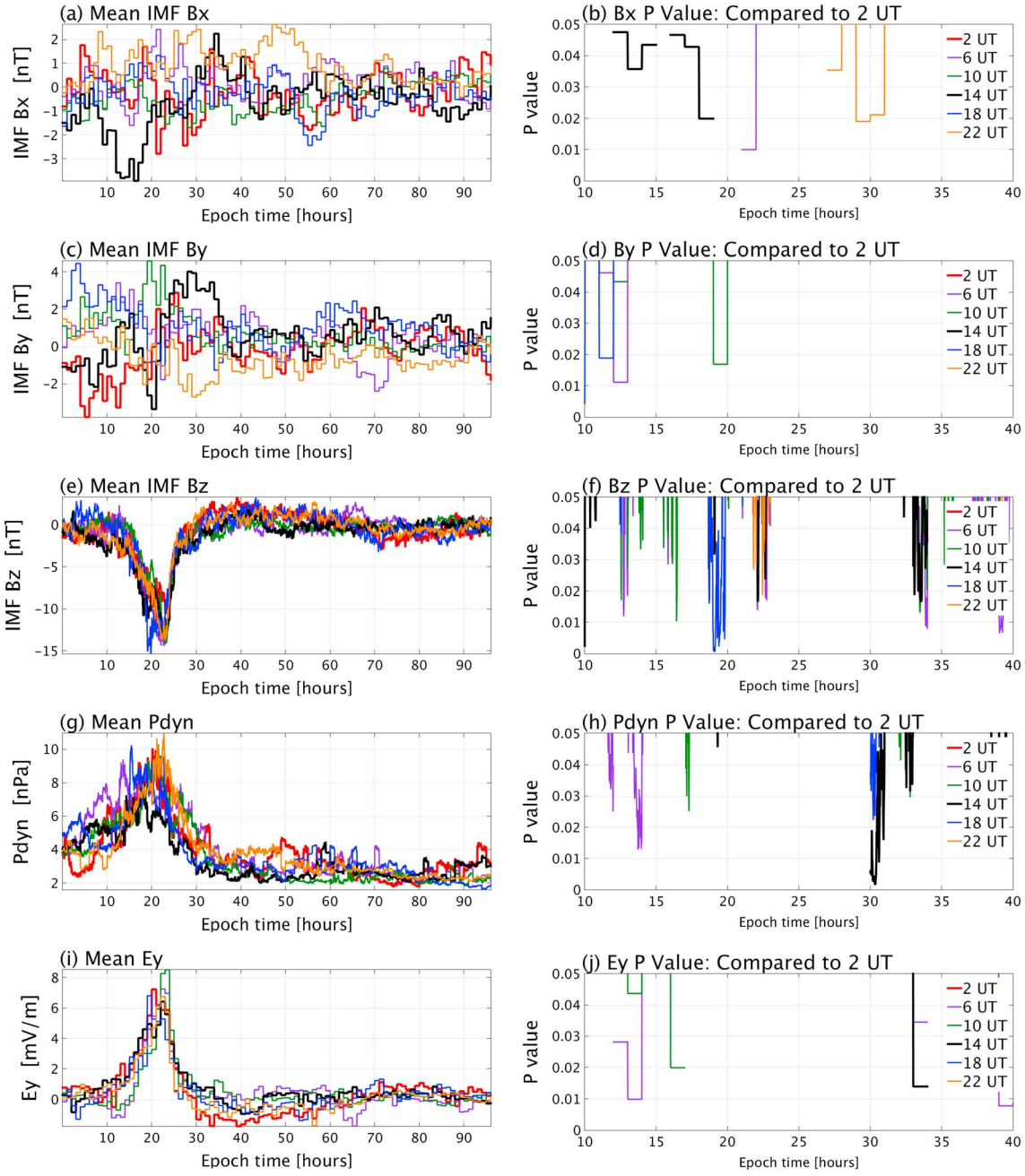

Figure 4. (a, c, e, g, and i) Mean IMF and solar wind values at each time step along the entire epoch timeline for each UT bin. (b, d, f, h, and j) The probability (*P*) that differences in the mean values along epoch time for each UT bin compared to 2 UT are due to random chance along a reduced epoch timeline (10–40) hours. The *P* values are only shown if they are less than 0.05 associated with $H = 1$ for each UT bin compared to each other.

have at least some time when the 2 UT *SYM-H* mean is significantly different compared to the other UT bin *SYM-H* mean value. This is especially true for the black curve, comparing the 2 UT bin with the 14 UT bin.

Figure 3 shows the *SYM-H P* values associated with $H = 1$ for each UT bin comparison. This figure extends the result shown in Figure 2 (only 2 UT) to include all UT bins. It also simplifies the statistics results by only showing the *P* value for times along the epoch timeline for which the means are statistically different.

The results presented in Figure 3 demonstrate that the mean *SYM-H* for each UT bin has some statistically significant differences from the other bins near peak times (24 h) while highlighting the large difference between each bin and 2 UT (largest storms) and 14 UT (smallest storms). While the plots redundantly show

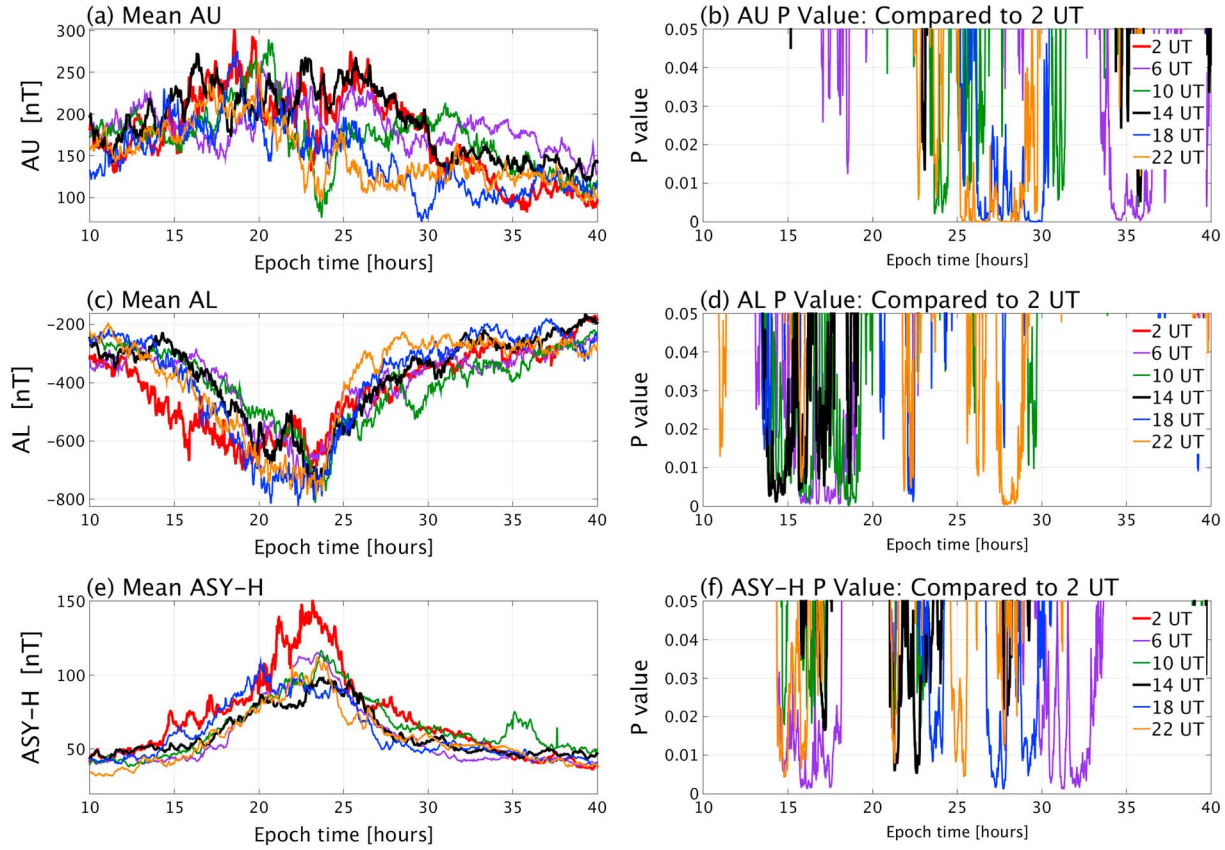

Figure 5. (a, c, and e) Mean values of magnetospheric indices at each time step along the reduced epoch timeline (10–40) hours for each UT bin. (b, d, and f) The probability (*P*) that differences in the mean values along the reduced epoch time for each UT bin compared to 2 UT are due to random chance. The *P* values are only shown if they are less than 0.05 associated with $H = 1$ for each UT bin compared to each other.

bin-to-bin comparisons, it clearly shows that the magnitude of the storms associated with each UT bin has some statistically significantly differences.

Figures 4a, 4c, 4e, 4g, and 4i show the mean IMF B_x, B_y, B_z, the solar wind dynamic pressure P_{dyn}, and electric field E_y for each UT bin along the epoch timeline (peak at 24 h). It should be noted that the B_x, B_y, and E_y are 1 h resolution, while the more important B_z, n, and P_{dyn} have 1 min resolution. From 15 to 35 h of epoch time the mean for the 2 UT bin (purple line) never exceeds the typical mean values of the other UT bins. In fact, the 18 UT bin appears to have the largest negative IMF B_z. Additionally, 18 UT and 6 UT have larger P_{dyn} than 2 UT.

Figures 4b, 4d, 4f, 4h, and 4j show the *P* values only during times for which the means are statistically different from the 2 UT bin. These values are sparse. For the comparison to B_x, the only notable difference is to 14 UT which (as Figure 4a shows) is due to 14 UT having much more negative B_x than any other UT bin. At first glance, more substantial differences occur for IMF B_z. But again, this is due to the more negative IMF B_z for the 18 UT bin, which would be expected to yield preference to stronger storms in the 18 UT bin but is not the case. Additionally, the difference highlighted in the P_{dyn} *P* value (Figure 4h) would be expected to give preference to stronger storms in the 6 UT bin. Therefore, this figure shows that any differences between 2 UT and the other UT bins are not due to solar wind conditions.

Figures 5a, 5c, and 5e display the mean of three additional magnetospheric indices used to describe storm progression: the upper auroral index *AU*, the lower auroral index *AL*, and the *H* component of the asymmetric index *ASY-H*. *AU* shows that convection for the 2 UT bin is within the standard range of all the other UT bins during the main phase (before ~24 h), although when comparing the 2 UT bin to 14 UT bin, the *AU* suggests weaker convection in the 2 UT bin, as was the case with the solar wind drivers. These differences are statistically significant in the 25–30 h epoch time.

The mean *AL* index and *ASY-H* index show enhanced activity and strong asymmetries during the main phase (approximately 12–19 h epoch time) for all UT bin storms. The 2 UT bin is apart from the other bins in both the *AL* and *ASY-H* indices in the early storm phase. Additionally, the mean *ASY-H* index shows a larger asymmetry in the 2 UT bin surrounding the peak of the storm (approximately 14–25 h epoch time) than the other UT bins. Both the differences in the *AL* and *ASY-H* indices are shown to be statistically significantly different using the *P* values when $H = 1$, as displayed in Figures 5b, 5d, and 5f.

5. Discussion

We studied the longitudinal dependence of the geomagnetic response to solar wind driving. To do this, we examined 305 storms subgrouped by the universal time of the storm peak as defined by *Dst*. We assessed each storm peak bin using several geomagnetic indices including *SYM-H*, $USGS_{Dst}$, *AU*, *AL*, and *ASY-H*. Analysis shows that the bin centered at 2 UT has significantly stronger events and the 14 UT bin significantly weaker. We considered each storm peak bin using IMF and solar wind parameters to confirm that any differences are not due to solar wind conditions. We now investigate possible origins for this phenomenon.

Typically, the storm strength is considered to be a function of the IMF and solar wind parameters [e.g., *Burton et al.,* 1975]. Contrary to this belief, Figure 4 shows that the 2 UT bin does not have a more negative IMF B_z or more enhanced solar wind data. In fact, the lines illustrating the mean values are overlapped and difficult to distinguish. In addition to the IMF, we also examined solar wind E_y and dynamic pressure and concluded that there were no significant differences between the means of the different UT bins that would drive the 2 UT bin storms more intensely than the other bins. Therefore, the stronger storms in the 2 UT bin are not driven by stronger solar wind conditions.

To further investigate the cause of the 2 UT storm enhancement, we examined several geomagnetic indices, including the *Dst*, *SYM-H*, $USGS_{Dst}$, *AU*, *AL*, and *ASY-H* indices. The major enhancement in the *ASY-H* index, seen in Figure 5, is controlled by interplay between three current systems that close through the ionosphere [cf. *Dubyagin et al.,* 2014]. This enhancement is attributed to extremely strong and/or frequent substorm activity, which is shown in the strong *AL* with minimum *AU* growth. To validate this result, we also examined and *t* tested the SuperMag auroral electrojet index (*SME*) along with the corresponding lower and upper envelopes *SML* and *SMU*. These indices are similar to the *AL* and *AU* indices, but the magnetometers differ in local time distribution. The *t* tests comparing the six UT bins for *AU* or SMU to the other UT bins show no statistical difference during the main phase. That is, the 2 UT bin is no different from any other UT bin when it comes to large-scale convection during the main phase. However, *t* tests comparing the 2 UT bin for *AL* or *SML* to the other UT bins are statistically different. That indicates that storms peaking in the 4 h window centered on 2 UT have a more enhanced *AL* throughout the main phase of the storm, implying that the storm time substorm intensity is UT dependent with a peak at 2 UT.

Several studies have examined the TEC diurnal and seasonal variation, but further study is required to investigate the consequences of this phenomenon on the magnetosphere's behavior. This result follows the study of *Lyatsky et al.* [2001], which found a preference to storms that peak between around 3–6 UT with less activity around 15–16 UT. In this study, we find that the magnitude of the storms in the 2 UT bin is more likely to be greater than any other group, particularly 14 UT regardless of equinoctial effects. Furthermore, we prove that this is not due to IMF or solar wind conditions. Rather, the effect appears to be caused by a tendency for enhanced substorm activity for the 2 UT bin.

Other bin sizes and time centering were explored. The shifting showed that the result was strongest with the current binning. The decrease in range resulted in significantly more uncertainty in the statistical results. Therefore, only one bin size choice and time centering choice were presented in the results above.

6. Conclusion

In this study we statistically examine the progression of intense geomagnetic storms grouped by the universal time (UT) of the peak *Dst*. We found that there is a demonstrable and significant UT dependence to the *Dst* peak of large storms. The storms that peak in the 4 h time bin centered on 2 UT are systematically more intense. They are especially more intense than events that peak 12 h later at 14 UT.

Several data sets were examined to determine the cause of the UT dependence. We showed that the solar wind drivers of each UT bin are not statistically different, indicating that the enhanced storm activity in the 2 UT time period is not driven by external factors. We also showed that the *AU* indices for each UT bin are not statistically different, which indicates that the large-scale dayside convection is statistically similar regardless of the UT timing of the storm peak—as was the case with the external drivers of the dayside convection.

The *AL* index during the storms is shown to have a UT dependence. This was validated using SML (not shown). Storms peaking near 2 UT have an enhanced *AL* throughout the main phase. Further, these storms are shown to be more asymmetric, most likely because of the enhanced substorm activity. This implies that the storm time substorm activity is UT dependent, with the peak in the activity occurring when the American Sector is near dusk.

Acknowledgments
The authors would like to thank NASA and NSF for sponsoring this work, in particular through grants NNX11A060G, NNX14AC02G, NNX16AG66G, AGS-1102863, AGS-1113478, and AGS-1414517. The authors would also like to thank the Kyoto World Data Center for providing access to the *Dst*, *SYM-H*, and *Kp* indices and NASA's CDA Web for providing access to the OMNI solar wind data.

References

Astafyeva, E., I. Zakharenkova, and M. Förster (2015), Ionospheric response to the 2015 St. Patrick's Day storm: A global multi-instrumental overview, *J. Geophys. Res. Space Physics*, *120*, 9023–9037, doi:10.1002/2015JA021629.

Barakat, A. R., J. V. Eccles, and R. W. Schunk (2015), Effects of geographic-geomagnetic pole offset on ionospheric outflow: Can the ionosphere wag the magnetospheric tail?, *Geophys. Res. Lett.*, *42*, 8288–8293, doi:10.1002/2015GL065736.

Burton, R. K., R. L. McPherron, and C. T. Russell (1975), An empirical relationship between interplanetary conditions and *Dst*, *J. Geophys. Res.*, *80*, 4204–4214, doi:10.1029/JA080i031p04204.

Coster, A. J., M. J. Colerico, J. C. Foster, W. Rideout, and F. Rich (2007), Longitude sector comparisons of storm enhanced density, *Geophys. Res. Lett.*, *34*, L18105, doi:10.1029/2007GL030682.

Crooker, N. U., and G. L. Siscoe (1974), Model geomagnetic disturbance from asymmetric ring current particles, *J. Geophys. Res.*, *79*, 589, doi:10.1029/JA079i004p00589.

Crooker, N. U., and G. L. Siscoe (1981), Birkeland currents as the cause of the low-latitude asymmetric disturbance field, *J. Geophys. Res.*, *86*, 11,201–11,210, doi:10.1029/JA086iA13p11201.

Davis, T. N., and M. Sugiura (1966), Auroral electrojet activity index *AE* and its universal time variations, *J. Geophys. Res.*, *71*, 785–801, doi:10.1029/JZ071i003p00785.

Dessler, A. J., and E. N. Parker (1959), Hydromagnetic theory of geomagnetic storms, *J. Geophys. Res.*, *64*, 2239–2252, doi:10.1029/JZ064i012p02239.

Dubyagin, S., N. Ganushkina, M. Kubyshkina, and M. Liemohn (2014), Contribution from different current systems to *SYM* and *ASY* midlatitude indices, *J. Geophys. Res. Space Physics*, *119*, 7243–7263, doi:10.1002/2014JA020122.

Dungey, J. W. (1961), Interplanetary magnetic field and the auroral zones, *Phys. Rev. Lett.*, *6*, 47–48, doi:10.1103/PhysRevLett.6.47.

Foster, J. C., A. J. Coster, P. J. Erickson, W. Rideout, F. J. Rich, T. J. Immel, and B. R. Sandel (2005), Redistribution of the stormtime ionosphere and the formation of the plasmaspheric bulge, in *Inner Magnetosphere Interactions: New Perspectives From Imaging*, edited by J. Burch, M. Schulz, and H. Spence, pp. 277–289, AGU, Washington, D. C.

Fukushima, N., and Y. Kamide (1973), Partial ring current models for worldwide geomagnetic disturbances, *Rev. Geophys.*, *11*, 795–853, doi:10.1029/RG011i004p00795.

Gannon, J. L., and J. J. Love (2011), USGS 1-min Dst index, *J. Atmos. Sol. Terr. Phys.*, *73*(2), 323–334.

Ganushkina, N., T. I. Pulkkinen, M. Liemohn, and A. Milillo (2006), Evolution of the proton ring current energy 670 distribution during April 21–25, 2001 storm, *J. Geophys. Res.*, *111*, A11S08, doi:10.1029/2006JA011609.

Ganushkina, N. Y., M. W. Liemohn, and T. I. Pulkkinen (2012), Storm-time ring current: Model-dependent results, *Ann. Geophys.*, *30*, 177–202, doi:10.5194/angeo-30-177-2012.

Gonzalez, W. D., J. A. Joselyn, Y. Kamide, H. W. Kroehl, G. Rostoker, B. T. Tsurutani, and V. M. Vasyliunas (1994), What is a geomagnetic storm?, *J. Geophys. Res.*, *99*, 5771–5792, doi:10.1029/93JA02867.

Gonzalez, W. D., B. T. Tsurutani, and A. L. Clua de Gonzalez (1999), Interplanetary origin of geomagnetic storms, *Space Sci. Rev.*, *88*, 529–562, doi:10.1023/A:1005160129098.

Greenspan, M. E., and D. C. Hamilton (2000), A test of the Dessler-Parker-Sckopke relation during magnetic storms, *J. Geophys. Res.*, *105*, 5419–5430, doi:10.1029/1999JA000284.

Huang, C. M. (2013), Disturbance dynamo electric fields in response to geomagnetic storms occurring at different universal times, *J. Geophys. Res. Space Physics*, *118*, 496–501, doi:10.1029/2012JA018118.

Immel, T. J., and A. J. Mannucci (2013), Ionospheric redistribution during geomagnetic storms, *J. Geophys. Res. Space Physics*, *118*, 7928–7939, doi:10.1002/2013JA018919.

Iyemori, T. (1990), Storm-time magnetospheric currents inferred from mid-latitude geomagnetic field variations, *J. Geomag. Geoelectr.*, *42*, 1249–1265, doi:10.5636/jgg.42.1249.

Iyemori, T., T. Araki, T. Kamei, and M. Takeda (1992), *Mid-Latitude Geomagnetic Indices ASY and SYM (provisional) No. 1 1989*, *Data Anal. Center for Geomag. and Space Magn.*, Kyoto Univ., Kyoto, Japan.

Jorgensen, A. M., H. E. Spence, W. J. Hughes, and H. J. Singer (2004), A statistical study of the global structure of the ring current, *J. Geophys. Res.*, *97*, A12204, doi:10.1029/2003JA010090.

Kamide, Y., and N. Fukushima (1971), Analysis of magnetic storms with DR-indices for equatorial ring current field, *Rep. Ionos. Space Res. Jpn.*, *25*, 125–162.

Katus, R., M. W. Liemohn, D. L. Gallagher, A. Ridley, and S. Zou (2013), Evidence for potential and inductive convection during intense geomagnetic events using normalized superposed epoch analysis, *J. Geophys. Res. Space Physics*, *118*, 181–191, doi:10.1029/2012JA017915.

Katus, R. M., and M. W. Liemohn (2013), Similarities and differences in low-to middle-latitude geomagnetic indices, *J. Geophys. Res. Space Physics*, *118*, 5149–5156, doi:10.1002/jgra.50501.

Liemohn, M. W. (2003), Yet another caveat to using the Dessler-Parker-Sckopke relation, *J. Geophys. Res., 108*(A6), 1251, doi:10.1029/2003JA009839.

Liemohn, M. W., and J. U. Kozyra (2003), Lognormal form of the ring current energy content, *J. Atmos. Sol. Terr. Phys.*, *65*, 871–886, doi:10.1016/S1364-6826(03)00088-9.

Love, J. J., and J. L. Gannon (2009), Revised Dst and the epicycles of magnetic disturbance: 1958-2007, *Ann. Geophys. Atmos. Hydro. Space Sci.*, *27*(8), 3101.

Lyatsky, W., P. T. Newell, and A. Hamza (2001), Solar illumination as cause of the equinoctial preference for geomagnetic activity, *Geophys. Res. Lett*, *28*, 2353–2356, doi:10.1029/2000GL012803.

Mandea, M., and M. Purucker (2005), Observing, modelling, and interpreting magnetic fields of the solid Earth, *Surv. Geophys.*, *26*(4), 415–459, doi:10.1007/s10712-005-3857-x.

Mayaud, P. N. (1980), *Derivation, Meaning, and Use of Geomagnetic Indices*, *Geophys. Monogr. Ser.*, vol. 22, 154 pp., AGU, Washington, D. C., doi:10.1029/GM022.

Newell, P. T., T. Sotirelis, J. P. Skura, C.-I. Meng, and W. Lyatsky (2002), Ultraviolet insolation drives seasonal and diurnal space weather variations, *J. Geophys. Res.*, *107*(A10), 1305, doi:10.1029/2001JA000296.

O'Brien, T. P., and R. L. McPherron (2000), An empirical phase space analysis of ring current dynamics: Solar wind control of injection and decay, *J. Geophys. Res.*, *105*, 7707–7719, doi:10.1029/1998JA000437.

Perlongo, N. J., and A. J. Ridley (2016), Universal time effect in the response of the thermosphere to electric field changes, *J. Geophys. Res. Space Physics*, *121*, 3681–3698, doi:10.1002/2015JA021636.

Russell, C. T., and R. L. McPherron (1973), Semiannual variation of geomagnetic activity, *J. Geophys. Res.*, *78*, 92–108, doi:10.1029/JA078i001p00092.

Saroso, S., T. Iyemori, and M. Sugiura (1993), Universal time variations in the *ap* and *Dst* indices and their possible cause, *J. Geomagn. Geoelectr.*, *45*(7), 563–572, doi:10.5636/jgg.45.563.

Sckopke, N. (1966), A general relation between the energy of trapped particles and the disturbance field near the Earth, *J. Geophys. Res.*, *71*, 3125–3130, doi:10.1029/JZ071i013p03125.

Sugiura, M., and T. Kamei (1991), Equatorial *Dst* index 1957–1986, *IAGA Bull. No*. 40, ISGI, Saint-Maur-des-fosses, France.

Turner, N. E., D. N. Baker, T. I. Pulkkinen, J. L. Roeder, J. F. Fennell, and V. K. Jordanova (2001), Energy content in the storm time ring current, *J. Geophys. Res.*, *106*, 19,149–19,156, doi:10.1029/2000JA003025.

Wanliss, J. A., and K. M. Showalter (2006), High-resolution global storm index: *Dst* versus *SYM-H*, *J. Geophys. Res.*, *111*, A02202, doi:10.1029/2005JA011034.

Weimer, D. R. (2004), Correction to "Predicting interplanetary magnetic field (IMF) propagation delay times using the minimum variance technique", *J. Geophys. Res.*, *97*, A12104, doi:10.1029/2004JA010691.

Weimer, D. R., D. M. Ober, N. C. Maynard, M. R. Collier, D. J. McComas, N. F. Ness, C. W. Smith, and J. Watermann (2003), Predicting interplanetary magnetic field (IMF) propagation delay times using the minimum variance technique, *J. Geophys. Res.*, *108*(A1), 1026, doi:10.1029/2002JA009405.